Article

Partial Oxidation of Methane to Syngas on Rh/Al$_2$O$_3$ and Rh/Ce-ZrO$_2$ Catalysts

Raquel L. Oliveira, Isabela G. Bitencourt and Fabio B. Passos*

*Departamento de Engenharia Química e Petróleo, Universidade Federal Fluminense,
Rua Passo da Pátria, 156, 24210-240 Niterói-RJ, Brazil*

A oxidação parcial do metano sobre catalisadores de ródio suportados em γ-Al$_2$O$_3$, CeO$_2$, ZrO$_2$ e Ce-ZrO$_2$ foi investigada. Medidas de DRIFTS (espectroscopia no infravermelho com reflectância difusa) de CO adsorvido mostraram que houve a formação de diferentes espécies de ródio nos diferentes suportes, o que por sua vez influenciou na dispersão do metal. Os efeitos da dispersão metálica e da capacidade de armazenamento de oxigênio sobre a atividade dos catalisadores na oxidação parcial foram discutidos.

The partial oxidation of methane with γ-Al$_2$O$_3$-, CeO$_2$-, ZrO$_2$- and Ce-ZrO$_2$-supported rhodium catalysts was investigated. DRIFTS (diffuse reflectance infrared spectroscopy) measurements of adsorbed CO showed the formation of different rhodium species on different supports, which influenced the dispersion of the metal. The effects of the metal dispersion, oxygen storage capacity on the activity of these catalysts for the partial oxidation of methane are discussed.

Keywords: methane partial oxidation, methane, ceria-zirconia, rhodium, DRIFTS

Introduction

The catalytic partial oxidation of methane is an alternative to steam reforming, the industrial process for the production of synthesis gas from methane. Partial oxidation is a more energy efficient and less expensive process than steam reforming. The partial oxidation of methane (POM) is a mildly exothermic reaction, in which methane reacts with a limited amount of oxygen to produce hydrogen and carbon monoxide:

$$CH_4 + \tfrac{1}{2} O_2 \rightarrow CO + 2H_2 \qquad (1)$$

The POM process is capable of producing syngas with a H$_2$/CO ratio of approximately 2, which makes it a favorable method for methanol and hydrocarbon synthesis.[1,2] Noble metal catalysts (Ir, Ru, Rh, Pt, Pd) exhibit high activity, along with long-term stability, while minimizing the levels of coking, particularly when compared to the non-noble metals (such as Fe, Co, Ni).[1,2] The lack of a hydrogen infrastructure, as well as disadvantages in hydrogen storage, has stimulated the development of compact fuel processors, which are able to produce a rich hydrogen gas mixture from hydrocarbons. Several studies have reported that Rh

catalysts are especially appropriate for use in compact fuel processors because of their high activity, selectivity for syngas and resistance to carbon deposition.[2]

One of the main disadvantages of methane conversion is the deactivation due to coke formation. Thus, there is a great interest in designing catalysts that minimize the deleterious effect of coking. The presence of oxygen vacancies in supports that contain CeO$_2$ proved to be instrumental in keeping the metal particles free from coke deposition during the steam reforming,[3-5] partial oxidation,[6-9] CO$_2$ reforming and autothermal reforming of methane,[10-12] when using nickel or noble metals as catalysts.[13-15] Furthermore, ceria may also improve the catalytic performance by increasing the noble metal dispersion and stabilizing the support. Both the metal dispersion and support reducibility of Pt/CeO$_2$ and Pt/Ce$_x$Zr$_{1-x}$O$_2$ were found to influence the catalytic activity and stability of the catalysts in the partial oxidation of methane.[6,10] An increase in the activity of Rh/CeZrO$_2$ for the partial oxidation of methane as a result of a higher Rh dispersion has also been reported.[11,12]

In this work, the effects of the support on the partial oxidation of methane were investigated further. Rh/γ-Al$_2$O$_3$, Rh/CeO$_2$, Rh/ZrO$_2$ and Rh/Ce-ZrO$_2$ catalysts were prepared and characterized by diffuse reflectance UV-Vis spectroscopy (DR-UV-Vis spectroscopy), temperature programmed reduction (TPR), X-ray diffractometry

*e-mail: fbpassos@vm.uff.br

(XRD), CO and H_2 chemisorption and diffuse reflectance infrared spectroscopy (DRIFTS) of adsorbed CO. The metal surface was also examined through the dehydrogenation of the cyclohexane model reaction. The partial oxidation of methane by these catalysts was investigated by temperature programmed surface reaction (TPSR) and the stability of the catalysts was probed in a continuous reactor.

Experimental

Catalyst preparation

The catalysts were prepared by incipient wetness using $Rh(NO_3)_3$ (final Rh content equal to 1.5%) as the precursor. γ-Al_2O_3, ZrO_2 and CeO_2 supports were obtained by calcining bohemite (Catapal), $(NH_4)_2Ce(NO_3)_6$ (Aldrich) and $Zr(OH)_2$ (Aldrich), respectively, at 800 ºC for 1 h. The $Ce_xZr_{1-x}O_2$ (x = 0.25, 0.5, 0.75) supports were obtained through a co-precipitation method.[13] An aqueous solution of $(NH_4)_2Ce(NO_3)_6$ (Aldrich) and $ZrO(NO_3)_2$ (Aldrich) was prepared to obtain the desired amounts of CeO_2 and ZrO_2. Then, the ceria and zirconium hydroxides were co-precipitated by the addition of excess NH_4OH (Merck). Finally, the precipitate was washed with distilled water and calcined at 800 ºC for 1 h.

Catalyst characterization

BET specific surface areas were measured at –196 °C in a Micromeritics ASAP 2010. The samples (1 g) were previously dried at 250 ºC under vacuum. TPR measurements were carried out in a micro-reactor coupled to a quadrupole mass spectrometer (Balzers, Omnistar). The samples (150 mg) were dehydrated at 150 ºC for 30 min under He flow prior to reduction. After cooling to room temperature, the samples were then subjected to 5% H_2/Ar gas flow (30 mL min^{-1}), and the temperature was raised to 1000 ºC at a rate of 10 ºC min^{-1}.

XRD data of the calcined catalysts, and their respective supports, were performed in a Rigaku Miniflex spectrometer using monochromatic Cu K_α (1.540 Å) radiation with a scan rate of 0.05 °C min^{-1} and a 2θ range of 2-90º.

In the literature, structure insensitive reactions have been reported for the characterization of catalysts.[14] The rhodium active phase was probed through cyclohexane dehydrogenation as a structure insensitive reaction.[14] This reaction was performed under atmospheric pressure in a continuous flow micro-reactor. The pretreatment of the samples (10 mg) consisted of drying them at 150 ºC under a stream of He (30 mL min^{-1}) for 30 min, followed by reduction at 500 ºC under a H_2 flow (10 ºC min^{-1}) and

a final purge using He (30 mL min^{-1}) at 800 ºC for 30 min. The reactant mixture was obtained by bubbling hydrogen through a saturator containing cyclohexane at 12 ºC (H_2/C_6H_{12} 13.6). The total flow rate was equal to 100 mL min^{-1} and the temperature was 270 ºC. The effluent gas phase was analyzed with an on-line gas chromatograph (HP-5890) equipped with a flame ionization detector and an HP Innowax capillary column. Under these conditions, no significant deactivation of the catalysts was observed, and there were no diffusional or thermodynamic limitations.

H_2 and CO chemisorption measurements were conducted using a Micromeritics ASAP 2010 gas sorption analyzer. The mass of the samples used was 500 mg. The calcined samples were subjected to a standard procedure consisting of heating the sample under He (30 mL min^{-1}) at 150 ºC for 30 min, followed by reduction in a flow of H_2 (30 mL min^{-1}) at a rate of 10 ºC min^{-1} up to 500 ºC. Then, the samples were heated in He (30 mL min^{-1}) to 800 ºC. Then, the samples were evacuated for 30 min at the final temperature to remove any residual H_2, before cooling under vacuum to 35 ºC for analysis. The irreversible H_2 and CO uptakes were obtained using the difference between total and reversible H_2 and CO uptakes. A chemisorption stoichiometry of H:Rh 1:1 and CO:Rh 1:1 was assumed.

DR-UV-Vis spectroscopy was carried out in a Varian model Cary 5.0 spectrometer equipped with a diffuse reflectance accessory (Harrick). To separate the contribution of the support, the reflectance R(λ) of the sample was made proportional to the reflectance of the respective support, and the Kubelka-Munk function F(R) was calculated.

In situ infrared spectra of the samples were conducted using a Bruker VERTEX 70 FTIR equipped with an LN-MCT detector, using a diffuse reflectance cell (Harrick, HVC-DRP-4) with ZnSe windows. The spectra were recorded at 4 cm^{-1} resolution with 256 scans for each spectrum in the range from 2200 to 1700 cm^{-1}. The samples were pretreated *ex situ* as described in the chemisorption experiments, and then passivated under a flow of 5% O_2/He for 15 min at room temperature. Before each experiment, the samples were reduced in the cell under a H_2 flow (30 mL min^{-1}) at 500 ºC for 1 h. After purging with He (30 mL min^{-1}) for 30 min at the reduction temperature, background interferograms were obtained at the following temperatures: 300, 200, 100 and 30 ºC. The samples were subsequently subjected to a 5% CO/He gas stream (30 mL min^{-1}) at room temperature for 1 h. The samples were purged with He for 1 h. Then, interferograms of the adsorbed CO were collected at each temperatures at which a background interferogram was taken. The absorbance spectrum was calculated from the ratio of the sample interferogram and to that of the background interferogram.

Partial oxidation of methane

The partial oxidation of methane was performed in a quartz reactor at atmospheric pressure. Prior to each reaction, the catalyst was reduced under a flow of H_2 (30 mL min^{-1}) at 500 ºC for 1 h and then heated to 800 ºC under a He flow (30 mL min^{-1}). The reaction was carried out at 800 ºC and weight hourly space velocity (WHSV) of 520 h^{-1} for all catalysts. A reactant mixture with a CH_4:O_2 ratio of 2:1 and a total flow rate of 100 mL min^{-1} was used. To avoid temperature gradients, catalyst samples (10 mg) were diluted with inert SiC (18 mg). The transfer lines were kept at 140 °C to avoid condensation. The exit gases were analyzed using a gas chromatograph (Varian CP3800) equipped with a thermal conductivity detector and a Carboxen 1010 capillary column (SUPELCO). The H_2 and CO selectivities were determined via the equations:

$$H_2 \text{ selectivity} = \frac{\text{mols of } H_2 \text{ out}}{\text{mols of } H_2 \text{ out} + \text{mols of } H_2O \text{ out}} \quad (2)$$

$$CO \text{ selectivity} = \frac{\text{mols of CO out}}{\text{mols of CO out} + \text{mols of } CO_2 \text{ out}} \quad (3)$$

The TPSR experiments were performed in the same apparatus used for the TPR measurements. After drying under He at 150 ºC, the samples (150 mg) were reduced under a flow of H_2 at 500 ºC for 1 h, purged with a flow of He at 800 ºC for 30 min, and cooled to room temperature. The samples were subjected to a flow of CH_4/O_2/He (2:1:27) at 30 mL min^{-1} while the temperature was raised to 800 ºC at rate of 20 ºC min^{-1}.

Results and Discussion

Catalyst characterization

BET specific surface areas of the several catalysts are shown in Table 1. As expected, the 1.5%Rh/γ-Al$_2$O$_3$ presented the highest surface area, followed by the mixed oxide supported Rh catalysts, which presented higher surface areas than the single CeO$_2$- and ZrO$_2$-supported catalysts.

Table 1. BET specific surface area and H$_2$ uptake during TPR for Rh catalysts

Catalyst	S_{BET} / (m^2 g^{-1})	H$_2$ uptake / (μmol g$_{cat}^{-1}$)
1.5%Rh/γ-Al$_2$O$_3$	188	1.9
1.5%Rh/CeO$_2$	16	4.1
1.5%Rh/ZrO$_2$	37	1.8
1.5%Rh/Ce$_{75}$Zr$_{25}$O$_2$	58	3.5
1.5%Rh/Ce$_{50}$Zr$_{50}$O$_2$	52	3.1
1.5%Rh/Ce$_{25}$Zr$_{75}$O$_2$	49	2.6

TPR profiles of the supports are presented in Figure 1. The CeO$_2$ support showed H$_2$ consumption peaks at approximately 490 and 810 ºC; usually these are ascribed to the reduction of the capping and bulk CeO$_2$ respectively.[15] No reduction was observed for γ-Al$_2$O$_3$ and ZrO$_2$.[16,17] Ce-ZrO$_2$ supports presented maximum temperatures of reduction that shifted from 602 to 549 ºC with increasing CeO$_2$ content. These peaks are related to the CeO$_2$ reduction in a solid Ce-ZrO$_2$ solution, which happened at a lower temperature than the reduction temperature observed for pure CeO$_2$.[18]
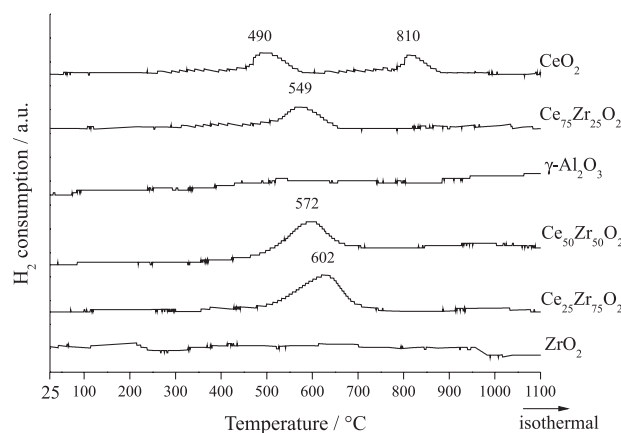
Figure 1. Temperature programmed reduction profiles of the Al$_2$O$_3$, CeO$_2$, ZrO$_2$ and Ce-ZrO$_2$ supports.

The TPR profile (Figure 2) for the 1.5%Rh/γ-Al$_2$O$_3$ catalyst showed a peak at 154 °C, which may be attributed to the reduction of Rh$_2$O$_3$.[19,20] The profile for the 1.5%Rh/CeO$_2$ catalyst showed peaks at 96, 224 and 967 °C. The first two peaks may be attributed to the reduction of well-dispersed Rh$_2$O$_3$ and of larger Rh$_2$O$_3$ particles,[21] which occurs simultaneously with the reduction of the surface ceria, and the last peak results from the reduction of bulk ceria.[22] For the 1.5%Rh/ZrO$_2$, there were peaks at 98 and 211 °C corresponding to the reduction of two different types of Rh$_2$O$_3$, one with high dispersion and the other with low dispersion.[23] The 1.5%Rh/Ce$_{75}$Zr$_{25}$O$_2$ TPR profile presented peaks at 98, 135, 238 and 1003 °C, which may be attributed to the reduction of well dispersed Rh$_2$O$_3$, larger Rh$_2$O$_3$ particles, surface ceria and the reduction of bulk ceria, respectively. Additionally, the TPR profiles of the 1.5%Rh/Ce$_{25}$Zr$_{75}$O$_2$ and 1.5%Rh/Ce$_{50}$Zr$_{50}$O$_2$ catalysts presented only two peaks, the first due to the reduction of well dispersed Rh$_2$O$_3$ and the second resulting from simultaneous reduction of Rh$_2$O$_3$ and the respective supports.[23] The hydrogen uptakes of the supported catalysts during the TPR experiments are displayed in Table 1 and are consistent with the previous peak assignments.
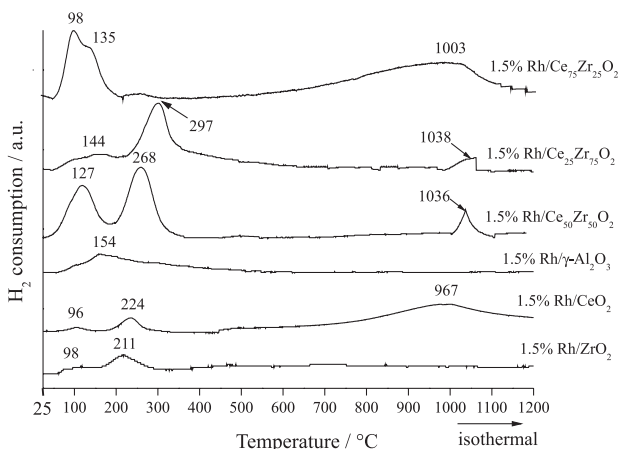
Figure 2. Temperature programmed reduction profiles of the 1.5%Rh/γ-Al$_2$O$_3$, 1.5%Rh/CeO$_2$, 1.5%Rh/ZrO$_2$ and 1.5%Rh/Ce-ZrO$_2$ catalysts.

Figure 3 shows the XRD patterns of the Rh catalysts. Due to the low Rh content and high dispersion,[2] no Rh$_2$O$_3$ peaks were detected. Thus, all catalysts presented diffraction patterns essentially identical to their respective supports.
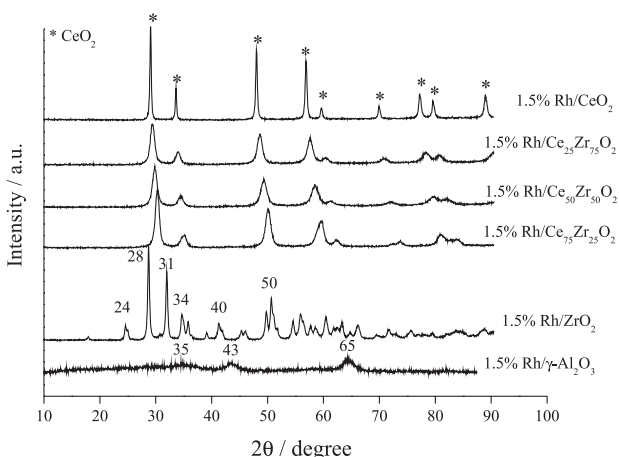
Figure 3. X-Ray diffraction patterns of the 1.5%Rh/γ-Al$_2$O$_3$, 1.5%Rh/CeO$_2$, 1.5%Rh/ZrO$_2$ and 1.5%Rh/Ce-ZrO$_2$ catalysts.

The 1.5%Rh/γ-Al$_2$O$_3$ catalyst showed the presence of peaks at approximately 2θ 45 and 70°, which are characteristic of γ-Al$_2$O$_3$ obtained through the calcination of bohemite.[24,25] For 1.5%Rh/CeO$_2$, it was possible to observe the diffraction patterns relative to that of CeO$_2$ with a fluorite structure (JCPDS 4-0593), while a monoclinic ZrO$_2$ phase (JCPDS 13-307) could be detected for the 1.5%Rh/ZrO$_2$ catalyst.[15,26] The diffraction pattern for 1.5%Rh/Ce$_{75}$Zr$_{25}$O$_2$ did not show separate phases for CeO$_2$ or ZrO$_2$. There was a shift in the corresponding CeO$_2$ peaks from 2θ 28.6, 33.1, 47.51 and 56.41° to 2θ 28.9, 33.3, 48.1 and 57.0°. This shift increased to higher Bragg angles as the ZrO$_2$ content was increased (1.5%Rh/Ce$_{25}$Zr$_{75}$O$_2$ and 1.5%Rh/Ce$_{50}$Zr$_{50}$O$_2$).

This shift is related to the formation of a solid solution of CeO$_2$ and ZrO$_2$ with a cubic structure.[27]

Figure 4 shows the DR-UV-Vis spectra of the catalysts. For 1.5%Rh/γ-Al$_2$O$_3$, a broad band centered at 320 nm was present. This band corresponds to the $^1A_{1g} \rightarrow {}^1T_{1g}$ transition.[28,29] The spectra for the 1.5%Rh/ZrO$_2$, 1.5%Rh/CeO$_2$ and 1.5%Rh/Ce ZrO$_2$ catalysts displayed two broad bands, one centered at approximately 260 nm due to Rh-O charge transfer and the other at approximately 320 nm due to the $^1A_{1g} \rightarrow {}^1T_{1g}$ transition.[35] These results are consistent with the TPR results as the broad bands are due to the inhomogeneity of the surface.
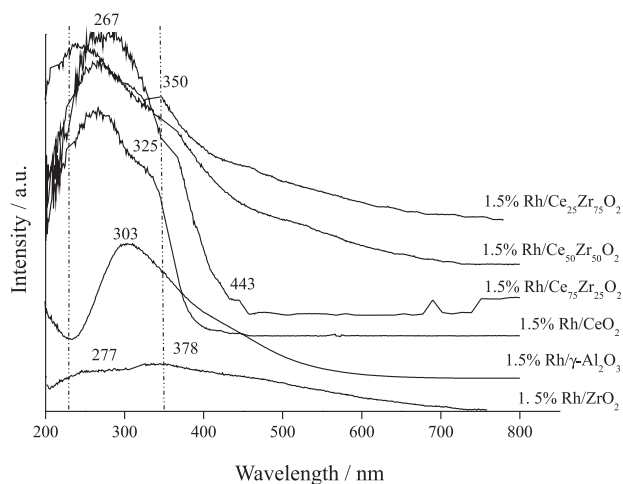
Figure 4. DRS-UV-Vis spectra of the 1.5%Rh/γ-Al$_2$O$_3$, 1.5%Rh/CeO$_2$, 1.5%Rh/ZrO$_2$ and 1.5%Rh/Ce-ZrO$_2$ catalysts.

Table 2 displays the results of H$_2$ and CO chemisorption on the catalysts. The 1.5%Rh/γ-Al$_2$O$_3$ catalyst showed larger H/Rh and CO/Rh values due to the higher γ-Al$_2$O$_3$ surface area. Rh/ZrO$_2$ presented the lowest H/Rh and CO/Rh ratios, although these values increase with CeO$_2$ content for the Rh/Ce-ZrO$_2$ catalysts. Since H$_2$ and CO can adsorb on CeO$_2$, these gases are not considered adequate to evaluate the dispersion of the CeO$_2$ supported catalysts.[30]

Additionally, cyclohexane dehydrogenation was used to probe the surface active sites of the investigated catalysts (Table 3). The initial dehydrogenation rate increased in the following order: 1.5%Rh/ZrO$_2$ < 1.5%Rh/Ce$_{50}$Zr$_{50}$O$_2$ < 1.5%Rh/CeO$_2$ < 1.5%Rh/Ce$_{75}$Zr$_{25}$O$_2$ < 1.5%Rh/Ce$_{25}$Zr$_{75}$O$_2$ < 1.5%Rh/γ-Al$_2$O$_3$.

DRIFTS absorption spectra of CO adsorbed on the catalysts at room temperature are displayed in Figure 5. The 1.5%Rh/γ-Al$_2$O$_3$ catalyst presented a major band with a maximum at 2090 cm^{-1} and a smaller band at 2019 cm^{-1}. These bands are associated with the symmetric and asymmetric CO stretching modes of the gem-dicarbonyl

Table 2. H_2 and CO chemisorption uptake at 35 ºC on Rh catalysts

Catalyst	CO uptake / ($\mu mol\ g_{cat}^{-1}$)		CO/Rh* / %	H_2 uptake / ($\mu mol\ g_{cat}^{-1}$)		H/Rh* / %
	Total	Irreversible uptake		Total	Irreversible uptake	
1.5%Rh/γ-Al$_2$O$_3$	120	98.5	67.6	58.1	36.5	50.1
1.5%Rh/CeO$_2$	25.7	24.3	16.7	22.8	12.8	17.6
1.5%Rh/ZrO$_2$	30.6	11.2	7.7	22.0	5.9	8.1
1.5%Rh/Ce$_{75}$Zr$_{25}$O$_2$	34.9	28.9	19.8	27.0	14.0	19.2
1.5%Rh/Ce$_{50}$Zr$_{50}$O$_2$	41.2	21.3	14.6	29.5	10.6	14.5
1.5%Rh/Ce$_{25}$Zr$_{75}$O$_2$	34.3	18.7	12.8	29.6	7.0	9.6

Table 3. Cyclohexane dehydrogenation on Rh catalysts at 270 ºC

Catalyst	Initial rate / ($10^{-3}\ mol\ h^{-1}\ g_{cat}^{-1}$)
1.5%Rh/γ-Al$_2$O$_3$	121.1
1.5%Rh/CeO$_2$	52.2
1.5%Rh/ZrO$_2$	40.5
1.5%Rh/Ce$_{75}$Zr$_{25}$O$_2$	62.9
1.5%Rh/Ce$_{50}$Zr$_{50}$O$_2$	51.2
1.5%Rh/Ce$_{25}$Zr$_{75}$O$_2$	64.8

species Rh^I-(CO)$_2$, which are generated by reaction of atomically dispersed rhodium particles with surface hydroxyl groups and CO.[37,38] An additional band at 2062 cm^{-1} was observed for 1.5%Rh/CeO$_2$. This band results from the linear adsorption of CO on metallic rhodium crystallite particles.[31,32] This is consistent with the presence of both well dispersed and larger Rh particles indicated by the TPR experiments. Additionally, two broad bands at 1850 and 1940 cm^{-1} were observed and are attributed to two types of bridge-bonded CO on the Rh^0 sites.[33] With 1.5%Rh/ZrO$_2$, the absorbance intensities were lower than observed for the other catalysts, and the bands relative to gem-dicarbonyl species (2090 and 2020 cm^{-1}) were much smaller as expected because of the low CO adsorption capacity observed for this catalyst. A broad band between 2000 and 2050 cm^{-1}, attributed to the linear adsorption of CO on Rh metal, and a small band at 1850 cm^{-1}, attributed to bridge-bonded CO, were observed.[34] The spectra of the Rh/CeZrO$_2$ catalysts contained very broad bands, indicating a non-uniform distribution of Rh particle sizes. For the 1.5%Rh/Ce$_{75}$Zr$_{25}$O$_2$ catalyst, a main broad band was observed at 2055 cm^{-1} due to linear CO-Rh adsorption, with a tail at 1950 cm^{-1}. A small band at 1850 cm^{-1} due to the two types of bridge-adsorbed CO was also observed. A small shoulder was observed at 2020 cm^{-1} indicating a superposition of the bands resulting from the gem-dicarbonyl species (2090 and 2020 cm^{-1}) and the broad band centered at 2055 cm^{-1}. Similar results were observed for the 1.5%Rh/Ce$_{50}$Zr$_{50}$O$_2$ and 1.5%Rh/Ce$_{25}$Zr$_{75}$O$_2$ catalysts.
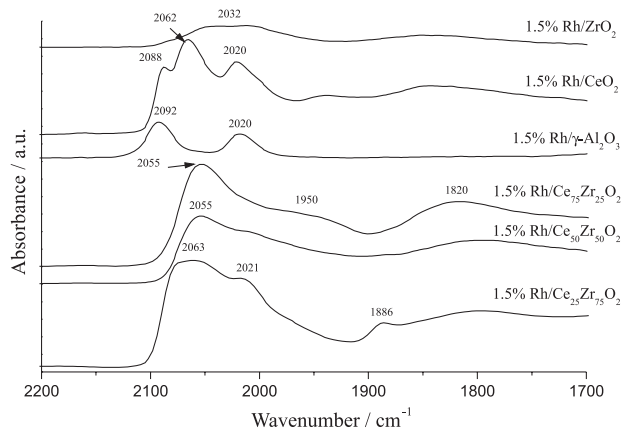
Figure 5. Infrared spectra of adsorbed CO at room temperature on 1.5%Rh/γ-Al$_2$O$_3$, 1.5%Rh/CeO$_2$, 1.5%Rh/ZrO$_2$ and 1.5%Rh/Ce-ZrO$_2$ catalysts.

Figure 6 shows the thermal desorption spectra for the 1.5%Rh/γ-Al$_2$O$_3$ catalysts. The intensity of the band relative to the gem-dicarbonyl species decreases as the temperature was raised. The frequencies of these bands were essentially invariant as is expected for CO adsorption on isolated sites.[37]

Conversely, 1.5%Rh/Ce$_{25}$Zr$_{75}$O$_2$ shows a decrease (Figure 7) in the frequency of the linearly bound CO from 2055 to 2028 cm^{-1} due to the decrease in the dipole-dipole
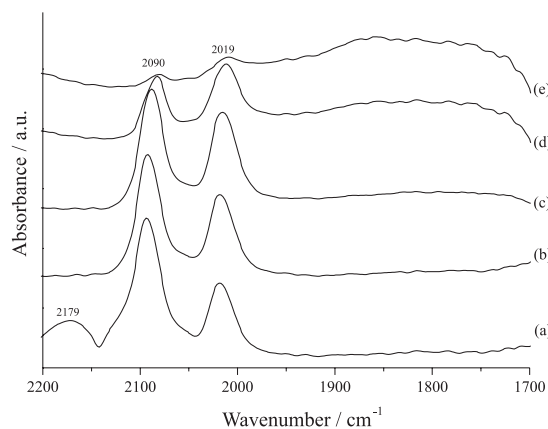
Figure 6. Thermal desorption infrared spectra of CO adsorbed on 1.5%Rh/γ-Al$_2$O$_3$, (a) under 10% CO/He flow at 30 °C, and under He flow at (b) 30, (c) 100, (d) 200 and (e) 300 °C.

interactions as CO coverage decreases. The bridge-bond CO was less stable to the temperature increase than the linearly adsorbed CO. Similar results were obtained for the other $Rh/CeZrO_2$ catalysts. These results confirm that the presence of Ce influences the state of Rh particles as reported by Erickson *et al.*[11]
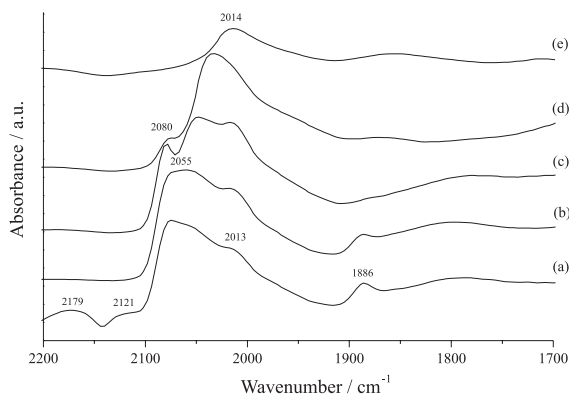
Figure 7. Thermal desorption infrared spectra of CO adsorbed on 1.5%$Rh/Ce_{25}Zr_{75}O_2$, (a) under 10% CO/He flow at 30 °C, and under He flow at (b) 30, (c) 100, (d) 200 and (e) 300 °C.

Partial oxidation of methane

Figure 8 shows the conversion of methane during the partial oxidation of methane using these catalysts. All of the catalysts showed an initial induction time, required to stabilize the actives sites, except for 1.5%Rh/γ-Al_2O_3. This may be because only 1.5%Rh/γ-Al_2O_3 presented isolated Rh atoms as indicated by the DRIFTS experiments. All of the catalysts were stable during the 24 h time-on-stream, and no coke could be detected by temperature programmed oxidation of the used catalysts. The order of activity (Table 4) approximated the same order observed for the H/Rh and CO/Rh chemisorption ratios, with 1.5%Rh/γ-Al_2O_3 presenting the highest conversion. Thus, the H_2 and CO chemisorption results were more reliable in predicting the order of methane conversion activity than the initial rate of cyclohexane dehydrogenation. This result is different than that observed for Pt/Ce-ZrO_2 catalysts, in which cyclohexane dehydrogenation provided good estimates for methane partial oxidation activity.[10]

The addition of cerium to ZrO_2 improved the activity of the Rh/Ce-ZrO_2 catalysts but only for molar ratios greater than 50%. The H_2 and CO selectivities for the catalysts followed the same trend as the activities (Figures 9 and 10).

The ratio of H_2/CO (Table 4) was close to a value of 2 for the catalysts, indicating that there was no influence from the reverse water gas shift reaction. X-ray Photoelectron (XPS) and IR spectroscopic studies have previously shown the complex nature of Rh/γ-Al_2O_3 for CPO, with Rh^0,
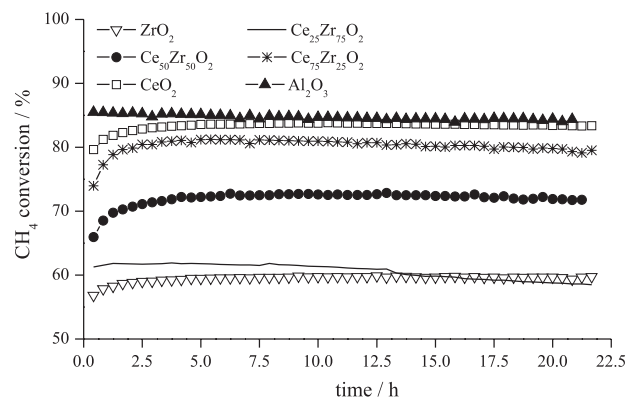
Figure 8. Methane partial oxidation on Rh catalysts (pressure: 1 atm, temperature: 800 °C and CH_4:O_2: 2:1, WHSV: 523 h^{-1}).

Table 4. Methane conversion and H_2/CO ratio obtained in the partial oxidation of methane on Rh catalysts (pressure: 1 atm, temperature: 800 °C and CH_4:O_2: 2:1, WHSV: 523 h^{-1})

Catalyst	CH_4 conversion / %	H_2/CO
1.5%Rh/γ-Al_2O_3	84.5	1.8
1.5%Rh/CeO_2	83.4	2.0
1.5%Rh/ZrO_2	60.0	1.9
1.5%$Rh/Ce_{75}Zr_{25}O_2$	80.4	2.0
1.5%$Rh/Ce_{50}Zr_{50}O_2$	72.0	2.1
1.5%$Rh/Ce_{25}Zr_{75}O_2$	59.0	2.1
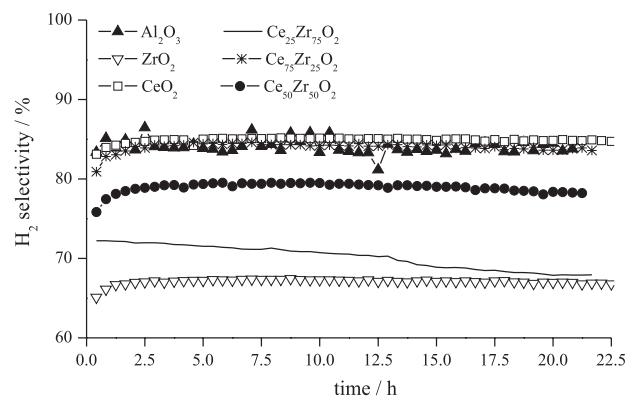
Figure 9. Selectivity to H_2 in the partial oxidation of methane on Rh catalysts (pressure: 1 atm, temperature: 800 °C and CH_4:O_2: 2:1, WHSV: 523 h^{-1}).

Rh^+ and Rh^{3+} coexisting on the surface under the reaction conditions.[11]

The TPSR results for all of the catalysts were consistent with an indirect mechanism for the partial oxidation of methane. Figure 11 shows a typical profile for the 1.5%$Rh/Ce_{25}Zr_{75}O_2$ catalyst, and the other samples showed similar profiles. In the beginning of the reaction, rhodium particles are covered by oxygen making the catalyst active for methane combustion. Then, the formation of CO and H_2 occurs through the CO_2 and H_2O reforming of methane. Several authors have also observed this indirect mechanism
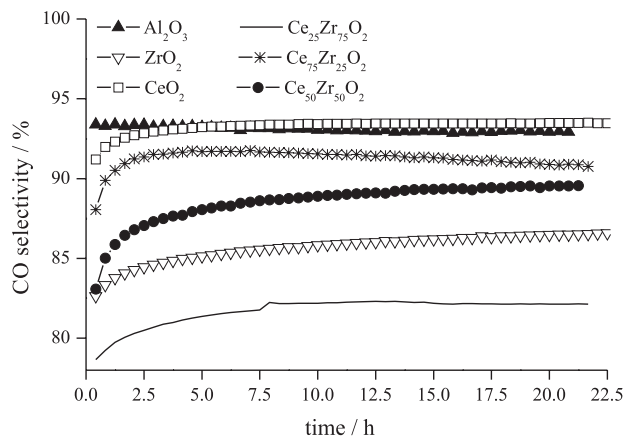
Figure 10. Selectivity towards CO in the partial oxidation of methane on Rh catalysts (pressure: 1 atm, temperature: 800 °C and CH_4:O_2: 2:1, WHSV: 523 h^{-1}).

with Pt/ZrO_2,[35] Pt/Ce-ZrO_2 and Rh/Ce-ZrO_2 catalysts.[16,17] In fact, recent theoretical and experimental results showed that the indirect mechanism is most probable for the catalytic partial oxidation of CH_4 as CO and H_2 are predominantly formed upon complete O_2 depletion from the sequential reforming steps.[42]
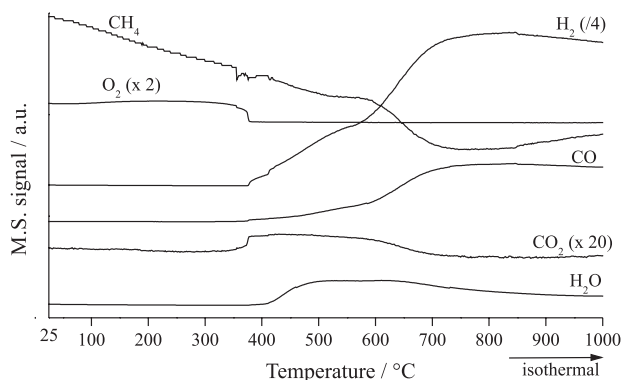
Figure 11. Temperature programmed surface reaction of methane partial oxidation using 1.5%Rh/$Ce_{25}Zr_{75}O_2$.

The advantage of using $CeZrO_2$ as a support has been explained by the continuous removal of carbonaceous deposits from the active sites at the metal-support interfacial perimeter.[6,11] However, under the reaction conditions used in this study, the catalysts have not been deactivated and the coke could not be detected by temperature programmed oxidation experiments. From this, an improvement in the dispersion for the Rh/$CeZrO_2$ catalysts when compared to Rh/ZrO_2 was the main observed effect.

Conclusions

Rhodium catalysts supported on γ-Al_2O_3, CeO_2, ZrO_2 and Ce-ZrO_2 were characterized and tested for the partial oxidation of methane to produce hydrogen. The formation of different rhodium species on the surface of different supports was evidenced by the DRIFTS measurements of adsorbed CO. The performance of Rh catalysts in the partial oxidation of methane was primarily dependent on the fraction of exposed metal. Rh/Ce-ZrO_2 showed better dispersion and consequently better catalytic activity compared to Rh/ZrO_2.

Reference

1. Tian, Z.; Dewaele, O.; Marin, G. B.; *Catal. Lett.* **1999**, *57*, 9.
2. Eriksson, S.; Nilsson, M.; Boutonnet, M.; Jaras, S.; *Catal. Today* **2005**, *100*, 447.
3. Laosiripojana, N.; Assabumrungrat, S.; *Appl. Catal., A* **2005**, *290*, 200.
4. Dong, W. S.; Roh, H. S.; Jun, K. W.; Park, S. E.; Oh, Y. S.; *Appl. Catal., A* **2002**, *226*, 63.
5. Purnomo, A.; Gallardo, S.; Abella, L.; Salim, C.; Hinode, H.; *React. Kinet. Catal. Lett.* **2008**, *95*, 213.
6. Mattos, L. V.; Oliveira, E. R.; Resende, P. D.; Noronha, F. B.; Passos, F. B.; *Catal. Today* **2002**, *77*, 245.
7. Xu, S.; Wang, X.; *Fuel* **2005**, *84*, 563.
8. Larrondo, S. A.; Kodjaian, A.; Fábregas, I.; Zimicz, M. G.; Lamas, D. G.; *Int. J. Hydrogen Energy* **2008**, *33*, 3607.
9. Salazar-Villalpando, M. D.; Reyes, B.; *Int. J. Hydrogen Energy* **2009**, *34*, 9723.
10. Passos, F. B.; de Oliveira, E. R.; Mattos, L. V.; Noronha F. B.; *Catal. Lett.* **2006**, *110*, 161.
11. Eriksson, S.; Rojas, S.; Boutonnet, M.; Fierro, J. L. G.; *Appl. Catal., A* **2007**, *326*, 8.
12. Boullosa-Eiras, S.; Zhao, T.; Chen, D.; Holmen, A.; *Catal. Today* **2011**, *171*, 104.
13. Hori, C. E.; Permana, H.; Simon, K. Y.; Brenner, A.; More, K.; Rahmoeller, M.; Belton, D.; *Appl. Catal., B* **1998**, *16*, 105.
14. Passos, F. B.; Frety, R.; Schmal, M.; *Catal. Lett.* **1992**, *14*, 57.
15. Roh, H. S.; Jun, K. W.; Dong, W. S.; Chang, J. S.; Park, S. E.; Joe, Y.; *J. Mol. Catal. A: Chem.* **2002**, *181*, 137.
16. Bozo, C.; Guilhaume, N.; Garbowski, E.; Primer, M.; *Catal. Today* **2000**, *59*, 33.
17. Dong, W. S.; Roh, H. S.; Jun, K. W.; Park, S. E.; Oh, Y. S.; *Appl. Catal., A* **2002**, *226*, 63.
18. Vidal, H.; Kašpar, J.; Pijolat, M.; Colon, G.; Bernal, S.; Cordo'n; *Appl. Catal., B* **2001**, *30*, 75.
19. Yao, H. C.; Japar, S.; Shelef, M.; *J. Catal.* **1977**, *50*, 407.
20. Hwang, C. P.; Yeh, C. T.; Zhu, Q.; *Catal. Today* **1999**, *51*, 93.

21. Van't, J. C.; Blik, H. F. J.; Huizinga, T.; Van Grondelle, J. V.; Prins, R.; *J. Catal.* **1985**, *95*, 333.

22. Diagne, C.; Idriss, H.; Kiennemann, A.; *Catal. Commun.* **2002**, *3*, 565.

23. Wang, J. A.; Lopez, T.; Bokhimi, X.; Novaro, O.; *J. Mol. Catal. A: Chem.* **2005**, *239*, 249.

23. Ruckenstein, E.; Wang, H. Y.; *J. Catal.* **1999**, *187*, 151.

25. Wang, S.; Lu, G. Q. M.; *Appl. Catal., B* **1998**, *16*, 269.

26. Pengpanich, S.; Meeyoo, V.; Rirksomboon, T.; Bunyakiat, K.; *Appl. Catal., A* **2002**, *234*, 221.

27. Hori, C. E.; Permana, H.; Simon, N. K. Y.; Brenner, A.; More, K.; Rahmoeller, K.M.; *Appl. Catal., B* **1998**, *16*, 105.

28. Lin, Q.; Shimizu, K.; Satsuma, A.; *Appl. Catal.*, A **2012**, *419*, 142.

29. Stoyanovskii, V. O.; Vedyagin, A. A.; Aleshina, G. A.; Volodin, A. M.; Noskov, A. S.; *Appl. Catal., B* **2009**, *90*, 141.

30. Rogemond, E.; Essayem, N.; Frety, R.; Perrichon, V.; Primet, M.; Mathis, F.; *J. Catal.* **1997**, *166*, 229.

31. Yang, A. C.; Garland, C. W.; *J. Phys. Chem.* **1957**, *61*,1504.

32. Rice, C. A.; Worley, S. D.; Curtis, C. W.; Guin, J. A.; Tarrer, A. R.; *J. Chem. Phys.* **1981**, *74*, 6487.

33. Kondarides, D. I.; Zhang, Z., Verykios, X. E.; *J. Catal.* **1998**, *176*, 536.

34. Gutierrez, A.; Karinen, R.; Airaksinen, S.; Kaila, R.; Krause, A. O. I.; *Int. J. Hydrogen Energy* **2011**, *36*, 8967.

35. Hegarty, M. E. S.; *Catal. Today* **1998**, *42*, 232.